Journal of Operation and Automation in Power Engineering
Vol. 5, No. 2, Dec. 2017, Pages: 191-203
http://joape.uma.ac.ir

Adaptive Observer-Based Decentralized Scheme for Robust Nonlinear Power Flow Control Using HPFC

*A. M. Shotorbani[1, 2, *], S. GhassemZadeh[1], B. Mohammadi-Ivatloo[1], S. H. Hosseini[1], L. Wang[2]*

[1]*Faculty of Electrical and Computer Engineering, University of Tabriz, Tabriz, Iran.*
[2]*School of Engineering, University of British Columbia, BC, Canada.*

Abstract- *This paper investigates the robust decentralized nonlinear control of power flow in a power system using a new configuration of UPFC. This structure comprises two shunt converters and one series capacitor called as hybrid power flow controller (HPFC). A controller is designed via control Lyapunov function (CLF) and adaptive observer to surmount the problems of stability such as tracking desired references, robustness against uncertainties, rejecting the disturbances, and remote data estimation. The suggested control scheme is decentralized using adaptive observer to estimate the non-local varying parameters of the system. Stability of the closed loop system is proved mathematically using Lyapunov stability theorem. Performance of the proposed finite-time controller (FT-C) is compared to another suggested exponentially convergent nonlinear controller (ECN-C) and a conventional PI controller (PI-C). Settling time of the state variables are diminished to a known little time by FT-C in comparison with ECN-C and PI-C. Simulation results are given to validate the proposed controllers. Effects of model uncertainties such as parameter variation in the transmission line and the converters are studied and properly compensated by the proposed controllers. The impact of the control gain and the communication time-delay is shown using the Bode diagram analysis.*

***Keywords*:** Decentralized control Lyapunov function, Flexible AC transmission systems, Hybrid power flow controller, Nonlinear control systems, Robust control.

1. INTRODUCTION

Employment of the FACTS devices in the modern power system, brings about low investment costs in comparison with building new power stations and expanding the transmission system [1]. It also ameliorates the system security, enhances the power transmission capabilities, and improves the reliability of the power grid [2]. Among FACTS devices, the unified power flow controller (UPFC) is the most capable element, which provides discriminate and appropriate regulation of impedance, phase angle, and power flow of a transmission line [3]. Different applications of UPFC are categorized as: control of power flow [2], voltage regulation [4], improving power system transients [5-7], and damping the low-frequency oscillation [8, 9]. Recent applications investigate the implementation of UPFC in wind farm integration [10-13], loss minimization [14], and improving the total transfer capability [15].

Received: 12 Nov. 16
Revised: 15 Mar. 17
Accepted: 20 Apr. 17
*Corresponding author:
E-mail: a.m.shotorbani@tabrizu.ac.ir (A. M. Shotorbani)
Digital object identifier: 10.22098/joape.2017.3007.1251

The conventional UPFC topology is combination of a shunt STATCOM and a series SSSC [2-7].

In view of power quality issues, the total harmonic distortion (THD) injected by the series converter is significant, in a wide range of operating points [16, 17]. In order to reduce the THD, some alternatives are investigated to resolve this deficiency such as: zigzag transformers and multilevel converters [18, 19]. Advantages of these solutions are discussed in the aforementioned references. A transformer-less configuration of UPFC is designed using cascaded multilevel converters [20-22], to eliminate zigzag transformers. It is shown that this configuration requires lower rating of the semiconductor devices, in connecting two synchronous ac systems with large phase difference [23], compared to the HVDC system using modular multilevel VSCs.

Moreover, a novel configuration of UPFC, named as hybrid power flow controller (HPFC) is presented recently in [16, 17] which uses two 3-phase shunt voltage source converters (VSCs) and a series capacitors.

The main advantage of the new configurations [16, 17] is its significant low THD of the voltage injected by the series capacitor, without using multilevel

VSCs. Besides, using two shunt VSCs simplifies the measuring and protection strategies [17] rather than UPFC. Moreover, the required rating of the second VSC is lower with HPFC in comparison with UPFC, for high active and reactive power flow. Nonetheless, the required rating for the second VSC of HPFC is higher when the power flow is near zero, which is not common in practice [17].

The VSCs of the HPFC [16, 17] are connected back-to-back with a common dc link. The HPFC is connected to the bus named as the sending end of the transmission line, as illustrated by v_s in Fig. 1.

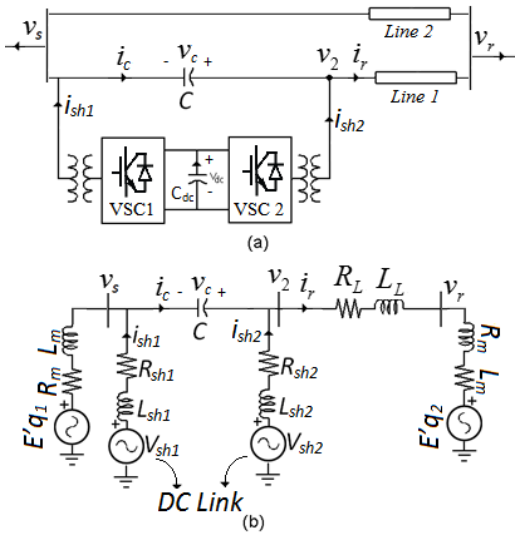

Fig. 1. (a) Schematic diagram of the HPFC in a power system with two parallel transmission lines, (b) Single phase representation of a power system with HPFC and equivalent model of the power grid

The existing UPFC power control schemes require fundamental modifications to be applicable to HPFC, due to structural differences. Despite UPFC, the investigations on the controller design for the HPFC are very limited.

Various techniques has been studied to design a power control scheme to the conventional UPFC, such as: control Lyapunov function (CLF) design [6, 24, 25], artificial neural network (ANN) [11], fuzzy ANN [12], fuzzy control [26], sliding mode control (SMC) [27], fuzzy SMC [12], feedback linearization [28, 29], adaptive backstepping design [30], backstepping with ANN-based approximation [31], optimal control [32, 33], structured singular value design [34], and robust H_2 control [35, 36].

Robustness of the linear controllers [32-34] is restricted to a limited neighborhood of the operating point, around which the system is linearized. However, disturbance rejection and robustness against parameter uncertainty are indispensable in practice [35-37]. In addition, fuzzy controllers require expert human knowledge, and ANN-based controllers need re-training and re-evaluating for robustness against parameter variations. The mentioned deficiencies deteriorate the control performance in the presence of large disturbances.

Furthermore, nonlinear controllers in [12, 26-31] as well as the linear controllers [32-35] lead to asymptotic convergence of state trajectories which have at least exponential or higher convergence rate. This means that the system's errors settle down with a large convergence time which is theoretically an infinite horizon. Nonetheless, finite-time controllers (FT-C) provide convergence of state trajectories in a pre-known finite time, and result in superior robustness against disturbances [38], compared to linear and nonlinear controllers which have exponential or asymptotic convergence.

Besides, robust nonlinear decentralized control of the HPFC has not been studied yet in the literature.

In addition, as it is shown in the following sections, the power flow control requires online and persistent measurement of the voltage at the ends of the transmission line, which requires a high-bandwidth communication infrastructure. This dependency weakens the system against large delays and communication loss. Using an adaptive observer, the control scheme is designed based on the local data, which eliminates the necessity for online and persistent communication of the remote measurements. The proposed decentralized observer-based control scheme, enhances the robustness of the system against communication delays and data losses.

In this paper, tow CLF-based controllers are proposed and applied to a power system with an HPFC. The proposed FT-C stabilizes the system in a specific known short time, rejects the disturbances, and makes the system robust against parameter uncertainties. Furthermore, the proposed controller is decentralized using an adaptive observer to estimate the remote data of the receiving end, which further eliminates the necessity for online persistent communication of the receiving end voltage. Decentralization of the controller, also enables using a communication infrastructure with a lower bandwidth, compared to the centralized control

scheme, in addition to the resiliency against communication delays, and data losses.

Remainder of the paper is organized as: steady state model of the HPFC is described in Section II. The CLF-based controllers are designed and stability of them are mathematically proved in section III. The adaptive observer is also introduced in section III. The simulation results are presented in Section IV. Finally, Section V concludes the paper.

2. MATHEMATICAL MODEL OF HPFC

As a new configuration, HPFC is built on two shunt VSCs and a capacitor connected in series. Fig. 1 depicts the schematic and the single-phase circuit diagram of an HPFC installed at the sending end of the transmission line. The sending and the receiving ends (i.e. v_s and v_r) are two busses of a multi-machine power system. The dynamics of the current of the transmission line in 'dq0' reference frame is calculated using the Park's transformation as:

$$\frac{d}{dt}\begin{pmatrix} i_{rd} \\ i_{rq} \end{pmatrix} = \frac{1}{L_L}\begin{pmatrix} -R_L i_{rd} + L_L \omega i_q - v_{rd} + v_{2d} \\ -R_L i_{rq} - L_L \omega i_d - v_{rq} + v_{2q} \end{pmatrix} \quad (1)$$

where R_L, L_L, i_r and v_r are resistance, inductance, current and receiving end voltage of the transmission line; v_2 is the voltage at the terminals of the second VSC's coupling transformer; $\omega = 2\pi f_0$, f_0 is the nominal system frequency; and the subscripts '*d*' and '*q*' represent the direct and quadrature axis components.

The current through the series capacitor is:

$$i_C = -C\frac{d}{dt}(v_2 - v_s) \quad (2)$$

where C is the series capacitor.

2.1. Nominal state space model of the VSCs

The *d-q* representation of the current through the VSC2 of the HPFC is:

$$\frac{d}{dt}\begin{pmatrix} i_{sh2d} \\ i_{sh2q} \end{pmatrix} = \frac{1}{L_{sh2}}\begin{pmatrix} -R_{sh2} i_{sh2d} + L_{sh2} \omega i_{sh2q} - v_{2d} + v_{sh2d} \\ -R_{sh2} i_{sh2q} - L_{sh2} \omega i_{sh2d} - v_{2q} + v_{sh2q} \end{pmatrix} \quad (3)$$

where v_{sh2}, i_{sh2}, R_{sh2}, and L_{sh2} are the injected voltage, current, resistance and inductance of the second shunt converter, respectively.

Obviously, the equations for the first shunt converter are the same as Eq. (3) with subscripts '1' which is excluded for brevity.

With respect to Eqs. (1)-(3), we present the state space model of two shunt VSCs as Eq. (4). This is the nominal model where the external disturbances and the perturbations are not considered.

$$\dot{x}(t) = Ax + Bu + v \quad (5)$$

where $x = [i_{sh1d}, i_{sh1q}, i_{sh2d}, i_{sh2q}]^T$ is the state vector; $u = [v_{sh1d}, v_{sh1q}, v_{sh2d}, v_{sh2q}]^T$ is the control vector; $B = diag\{1/L_{sh1}, 1/L_{sh1}, 1/L_{sh2}, 1/L_{sh2}\}$ is the input matrix; $v = B[v_{sd}, v_{sq}, v_{2d}, v_{2q}]^T$ is the grid voltage vector, and A is the state matrix as:

$$A = -B\begin{bmatrix} R_{sh1} & -L_{sh1}\omega & 0 & 0 \\ L_{sh1}\omega & R_{sh1} & 0 & 0 \\ 0 & 0 & R_{sh2} & -L_{sh2}\omega \\ 0 & 0 & L_{sh2}\omega & R_{sh2} \end{bmatrix}$$

The references for the transmitted power and the bus voltage are periodically updated by the upper control hierarchy. The current references of the transmission line are calculated considering the desired values of the transmitted active and reactive powers P_r^* and Q_r^* as:

$$i^*_{rd} = \frac{2}{3}\frac{P_r^* v_{rd} + Q_r^* v_{rq}}{v^2_{rd} + v^2_{rq}},\ i^*_{rq} = \frac{2}{3}\frac{P_r^* v_{rq} - Q_r^* v_{rd}}{v^2_{rd} + v^2_{rq}} \quad (6)$$

where superscript * denotes the reference value.

Then, the reference currents of the second shunt converter are:

$$i^*_{sh2d} = i_{rd}{}^* - i_{Cd},\ i^*_{sh2q} = i_{rq}{}^* - i_{Cq} \quad (7)$$

2.2. State space model of the VSCs considering external disturbances and perturbations

By defining the state tracking error as $e_i = x_i^* - x_i$, dynamics of the perturbed system including disturbances and uncertainties is calculated as:

$$\dot{e} = \dot{x}^* - \dot{x} = \dot{x}^* - Ax - v - Bu - g(t,x) \quad (8)$$

where $g(t,x) = [g_1, g_2, g_3, g_4]^T$ is a continuous norm-bounded function vector (i.e., $\| g(t,x) \| \leq g_m$, $g_m \in \mathbb{R}$) that aggregates the external disturbances, parameter uncertainties and variations, and the modeling errors [38] (See Appendix A.).

The dynamics of the dc link between two back-to-back VSCs is calculated by neglecting the power losses of VSCs as:

$$P_{dc} = P_{sh1} + P_{sh2} = v_{dc} i_{dc} = v_{dc}\left(-C_{dc}\dot{v}_{dc}\right) \quad (9)$$

where the subscripts dc, $sh1$, and $sh2$ are for the dc link, the first and the second VSCs, respectively; C_{dc} is the dc link capacitor; v_{dc} and i_{dc} are the dc link voltage and current as in Fig. 1 (a).

The current control loops of the VSCs of the HPFC, may employ the same controller developed for the converters of the conventional VSC-UPFC. However, the model order of the HPFC system is higher than the order of the conventional UPFC structure, due to the presence of the series capacitor in HPFC. Therefore, the power control loop of the HPFC has a different scheme compared to the UPFC. Although, advanced controllers can be used for the power control loop, a simple current-controlled scheme with feed-forward power control is proposed in this paper.

3. DESIGNING A FINITE TIME CONTROL LYAPUNOV FUNCTION

In this section, we design a robust finite-time control strategy using the CLF. First, the necessary definitions and Lemmas are provided. Then, the stability of the proposed controller is proved based on the Lyapunov theorem.

Definition 1. [39] Assume $f: D \to \mathbb{R}^n$ be a continuous function on $x \in D$ containing the origin, and suppose a nonlinear system as (10). The origin is a locally finite-time stable equilibrium, if the origin is Lyapunov stable and the solutions converge in a finite time.

$$\dot{x} = f(x),\ f(0) = 0, x \in \mathbb{R}^n \quad (10)$$

Lemma 1. [38] Assume there exist a Lyapunov function $V(x): D \to \mathbb{R}$ for system Eq. (10) such that;

$$V(x) + \gamma V^{\eta}(x) \le 0, \forall x \in D \quad (11)$$

where $\{p > 0, 0 < \eta < 1\} \in \mathbb{R}$, then the origin of Eq. (10) is a locally finite time stable equilibrium, and if $D = \mathbb{R}^n$ and V is radially unbounded, then the origin is a globally finite time stable equilibrium and the settling time of the states satisfies:

$$T(x_0) \le V^{1-\eta}(x_0) / \left(\gamma(1-\eta)\right) \quad (12)$$

Lemma 2. For $a, b, r \in \mathbb{R}$ we have:

$$\left(|a| + |b|\right)^r \le |a|^r + |b|^r,\ 0 < r < 1 \quad (13)$$

3.1. Finite-time CLF design for HPFC

For brevity, only the design approach for the controller of the second converter is fully described in the following. Obviously, the controller of the first converter is designed in the same way.

Statement 1. The system Eq. (8) with the control law Eq. (14) is finite-time stable, is robust against uncertainty and rejects bounded disturbances.

$$\begin{aligned} u^*_{sh2d} &= -R_{sh2} e_3 + R_{sh2} i^*_{sh2d} - L_{sh2}\omega i_{shq} + v_{2d} + \rho_3 g_m s_3 + \mu_3 e_3 \\ u^*_{sh2q} &= -R_{sh2} e_4 + R_{sh2} i^*_{sh2q} + L_{sh2}\omega i_{shd} + v_{2q} + \rho_4 g_m s_4 + \mu_4 e_4 \end{aligned} \quad (14)$$

where $s_i = sign(e_i)$ and $\rho_i, \mu_i, g_m > 0 \in \mathbb{R}$ are some real positive constants.

Proof. The proof is based on the Lyapunov stability theorem and Lemma 1. Assume a positive definite Lyapunov function:

$$V = L_{sh1}|e_1| + L_{sh1}|e_2| + L_{sh2}|e_3| + L_{sh2}|e_4| \quad (15)$$

Considering $\frac{d}{dt}(|e|) = \dot{e}_i s_i$, $e \neq 0$, we have:

$$\dot{V} = L_{sh1}\dot{e}_1 s_1 + L_{sh1}\dot{e}_2 s_2 + L_{sh2}\dot{e}_3 s_3 + L_{sh2}\dot{e}_4 s_4 \quad (16)$$

Substituting Eq. (8) into Eq. (16) yields:

$$\begin{aligned} \dot{V} &= L_{sh1}\dot{e}_1 s_1 + L_{sh1}\dot{e}_2 s_2 \\ &-\left(v_{sh2d} + R_{sh2} e_3 - R_{sh2} i^*_{sh2d} + L_{sh2}\omega i_{shq} - v_{2d} - L_{sh2} g_3\right) s_3 \\ &-\left(v_{sh2q} + R_{sh2} e_4 - R_{sh2} i^*_{sh2q} - L_{sh2}\omega i_{shd} - v_{2q} - L_{sh2} g_4\right) s_4 \end{aligned} \quad (17)$$

Substituting the proposed controllers Eq. (18) into v_{sh2d} and v_{sh2q} in Eq. (17), yields:

$$\dot{V} = -\sum_{i=1}^{4}\left(b_i g_i + \rho_i g_m s_i + \mu_i e_i\right) s_i \quad (19)$$

where $\rho_i, \mu_i, g_m > 0 \in \mathbb{R}$ are real positive constants.

Considering that the uncertainty function is norm-bounded (i.e. $\|g_i(t,x)\| \le g_m, i = 1,...,4$) and regarding $sign^2(e) = 1$ we conclude (20) for $\rho_i \ge b_i$.

$$\dot{V} \le -\sum_{i=1}^{4} \mu_i |e_i| \le 0 \quad (20)$$

The inequality (21) express the asymptotic stability of the system, with respect to Lyapunov theorem. In addition to (22), we have to establish the inequality (11) to get finite-time convergence. Therefore, the FT-C law is proposed as:

$$\begin{aligned} v^*_{sh2d} &= u^*_{sh2d} + \beta_3 sig^{\alpha}(e_3) \\ v^*_{sh2q} &= u^*_{sh2d} + \beta_4 sig^{\alpha}(e_4) \end{aligned} \quad (23)$$

where $\beta_i > 0 \in \mathbb{R}, i = 1...4$ are positive real constants;

v_{sh2d} and v_{sh2q} are defined as Eq. (14) and $sig^{\alpha}(e)=|e|^{\alpha}\,sign(e)$.

Substituting Eq. (23) into Eq. (17), considering lemma 2 and choosing $\beta=\min\{\beta_i\}$ we conclude:

$$\begin{aligned}\dot{V} &\le -\sum_{i=1}^{4}\left(\mu_i|e_i|+\beta_i|e_i|^{\alpha}\right)\\ &\le -\sum_{i=1}^{4}\beta_i|e_i|^{\alpha} \le -\beta V^{\alpha}\end{aligned} \tag{24}$$

From Lemma 1, we conclude that the system Eq. (8) with the proposed FT-C law Eq. (23) is finite-time stable and the convergence time T satisfies:

$$T(x_0)\le V^{1-\alpha}(x_0)/\left(\beta(1-\alpha)\right) \tag{25}$$

As a result, the proof is complete. In this paper, the proposed controller of Eq. (14) is called as the exponentially convergent nonlinear controller (ECN-C) and the control law Eq. (23) is named as FT-C. Obviously the controller for the first converter (i.e. v_{sh1d}^{*}, v_{sh1q}^{*}) are derived in the same way.

Remark 1: Settling time T is directly related to β^{-1}, i.e., larger β causes shorter T as indicated in (26). On the contrary, β directly affects control signals magnitude as in Eq. (27) and thus larger β leads to larger control output and higher consumed control energy. Designer should consider T and $\|u\|$ to be not very large in magnitude by selecting suitable β.

3.2. Chattering elimination

Chattering phenomena could occur in FT-Cs, since un-modeled fast electrical dynamics could be excited [40]. The design of the controller based on the reduced-order model of the plant, and application of this controller to the full-order plant would also cause unwanted chattering [41]. Chattering may lead to fatigue, vibrations, and attrition of mechanical devices in the power system. There have been some solutions to avoid chattering such as: high order sliding mode controllers (SMC) [39, 41], super-twisting SMC [42], and continuous approximation of the discontinuity [39].

In this paper, the discontinuity is removed by applying the approximation of Eq. (28) into Eq. (23). It yields a continuous and chattering-free controller.

$$sign(\xi)\approx \tanh(\varepsilon\times\xi),\ \xi\in\mathbb{R} \tag{28}$$

where $\varepsilon>0$ is a real constant.

From Eq. (28) it is perceived that although a large value of ε leads to a better approximation, it may also increase the occurrence possibility of chattering. Thus, a suitable value should be selected for ε by each specific design.

3.3. Decentralization of the proposed controller

In this section, an adaptive observer is employed to estimate the nominal value of non-locally measured parameter; the receiving end voltage (v_r). It is worth mentioning that v_r is not a state variable and state observers are futile in this case. Assume Eq. (1) is written in the form of:

$$\dot{z}=A_{obs}z+g+\Phi\theta \tag{29}$$

where $\theta=[v_{rd},v_{rq}]^T$ is the unknown parameters' vector; $z=[i_{rd},i_{rq}]^T$ is the observer state vector; $g=L_L^{-1}[v_{2d},v_{2q}]^T$ is the vector of the known terms; $\Phi=-L_L^{-1}I_{2\times2}$ and:

$$A_{obs}(u,y)=-\begin{bmatrix}R_LL_L^{-1} & -\omega\\ \omega & R_LL_L^{-1}\end{bmatrix}$$

It is supposed that the vector values z and θ are norm-bounded and z is locally available. An adaptive observer is proposed to estimate the remote receiving end voltage θ as [43]:

$$\begin{cases}\dot{\hat{\theta}}=mS_{\theta}^{-1}\Lambda^T(z-\hat{z})\\ \dot{\hat{z}}=A_{obs}\hat{z}+g+\Phi\hat{\theta}+m\left(\Lambda S_{\theta}^{-1}\Lambda^T+S_x^{-1}\right)(z-\hat{z})\end{cases} \tag{30}$$

where $\hat{z}$ and $\hat{\theta}$ are the vectors of the observed line current and the estimated receiving end voltages; S_x, S_θ and Λ are time-varying 2×2 real matrices with positive initial values; ρ_x,ρ_θ and m are constant positive scalars which determine the convergence speed. The adaption laws to update S_x, S_θ and Λ are given as:

$$\begin{cases}\dot{\Lambda}=\left(A_{obs}-mS_x^{-1}\right)\Lambda+\Phi\\ \dot{S}_x=-\rho_xS_x-A_{obs}^TS_x-S_xA_{obs}+mI_{2\times2}\\ \dot{S}_\theta=-\rho_\theta S_\theta+m\Lambda^T\Lambda\end{cases} \tag{31}$$

where $I_{2\times2}$ is the identity matrix.

The main objective of UPFC/HPFC is to expand the feasible operational area of the power system by increasing the controllability and flexibility of a

power transmission line. For a multi-machine power system, a UPFC is able to control the power flow through the transmission line, at which the UPFC is installed. The power flow between other busses of a multi-machine power system is principally influenced by the bus voltage phases and magnitudes. However, application of UPFC to alter the power flow in remaining transmission lines of the multi-machine power system, requires a higher-level control hierarchy and wide area measurements. Otherwise, the system in Fig. 1, representing two arbitrary busses of a multi-machine power system, is prevailing for power flow analysis.

In this paper, the power control loop and the HPFC current regulator are designed. It is assumed that the reference power through the transmission line is updated regularly by the authorized higher control level, such as the operator of the transmission system and the control center. Then, the proposed robust controller can be used to effectively control the power flow through the intended transmission line of the multi-machine power system.

Considering the proposed controllers and the adaptive observer, Fig. 2 depicts the HPFC power control scheme. In Fig. 2, the current calculator block, as the feed-forward power control loop, consists Eqs. (6) and (7). The current regulator block was designed in sections III-*A* and *B* whereas the observer block was proposed in section III-*C*.

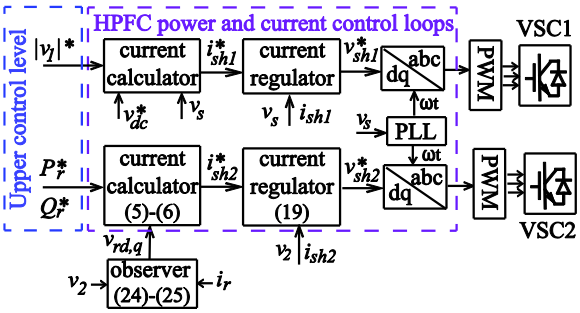

Fig. 2. Proposed decentralized control diagram for HPFC using adaptive observer and local measurements.

4. NUMERICAL SIMULATION

Capabilities of the suggested controllers are evaluated through MATLAB in a power system shown in Fig.1 to evaluate convergence and robustness. The ODE23 is selected with type of fixed step as the solver. The inverse of matrices for the proposed observer are calculated using LDL factorization. The studied system is perturbed and its parameters are corrupted by uncertainties since robustness of the nonlinear power system is extremely vital in practice.

As shown in Fig. 1, the test system is a two-bus power grid, where the HPFC is installed at one of the two parallel transmission lines. Since the power flow control is the objective, the reduced-order model of the machines used as an equivalent synchronous voltage source behind the series synchronous reactance [44].

Simulation parameters of HPFC and the proposed controller are presented in Tables I and II, respectively. The base voltage and power of the system are 100 (MVA) and 65 (kV), respectively.

In order to study the robustness capability of the proposed controllers, parameters of the controllers are set to nominal values (2nd column of Table I) while parameters of perturbed power system is set to simulation values which are 110% of the nominal values (3rd column of Table I) in the simulation.

The parameters of the proposed adaptive observer are given in Table III. The initial values of adaptation gain matrices in $S_\theta(0)$, $S_x(0)$, and $\Lambda(0)$ are set to the identical matrix.

Table 1. Parameters of HPFC in per-unit

Parameters	Nominal Values (pu)	Perturbed Simulation Values (pu)
R_{sh}	0.015	0.0165
X_{sh}	0.15	0.165
R_L	0.05	0.055
X_L	0.25	0.275
$1/(\omega C_{dc})$	0.5	0.55
C	3×10^{-6}	3.3×10^{-6}

Table 2. Parameters of the proposed FT-C and PI-C

parameter	ρ_i	μ_i	β_i	α	ε	*VSC #1*		*VSC #2*	
						K_p	K_I	K_p	K_I
value	1	1	1	7/9	30	0.27	61.3	0.3	65.6

Table 3. Parameters of the adaptive observer

Parameter	ρ_x	ρ_θ	m
Values	1e6	1e6	100

Two scenarios are simulated; first, the reference tracking capability of the proposed controllers are assessed in a perturbed system with parameter variation and average-value model of the VSCs. Second, the detailed model of back-to-back 3-level VSCs is employed to evaluate the proposed controllers when a short-circuit fault occurs at the middle of the second transmission line in Fig. 1.

4.1. Scenario 1 (decentralized reference tracking)
In order to challenge the robustness of the proposed controller in tracking the references, the receiving end real power reference is changed from initial value of 0.8 (pu) to 1.2 and 1.0 at *t=0.1* (s) and *t=0.3* (s), respectively. Simultaneously, reactive reference power is altered from initial value of -0.5 (pu) to -0.8 and to zero. The power angle between the sending and receiving ends generators, δ, is changed from -5 degree to +5 at *t=0.5* (s).

In all cases, the parameters of the power system are perturbed by +10% of their nominal values (See Table I and (34)) except for PI-C. Nonetheless, the proposed FT-C is able to compensate the uncertainties which is proved mathematically and will be evaluated numerically. Performance of the proposed FT-C is compared with the ECN-C (14), and with PI-C using the parameters in Table II.

The simulation results for the power flow control are given in Fig. 3. The settling time, and the transient overshoot are enhanced with the proposed FT-C, in comparison with ECN-C and PI-C. FT-C also yields lower overshoot magnitude and has diminished the interaction between real and reactive powers, as illustrated in Fig. 3.

The state variables and the controller outputs are shown in Figs. 4 and 5, respectively. The range of the currents and voltages in Figs. 4 and 5, prove that the states and the range of control signals are feasibly bounded and are in a practical range.

The VSC1 regulates the dc link voltage and the sending-end voltage magnitude, whereas the VSC2 regulates the current injected to the grid.

In order to compare the accuracy of the proposed controllers, the performance measures including mean integrated squared error (i.e. $MISE = h(e^2)$), mean integrated absolute error (i.e. $MIAE = h(|e|)$), and time-weighted *MIAE* (i.e. $MITAE = h(t|e|)$) are used, in which the function $h(\xi)$ is defined as [45]:

$$h(\xi) = \frac{1}{t_d}\int_{t_d} \xi(t)\,dt \qquad (32)$$

where t_d is the time duration, and e is the error Eq. (8).

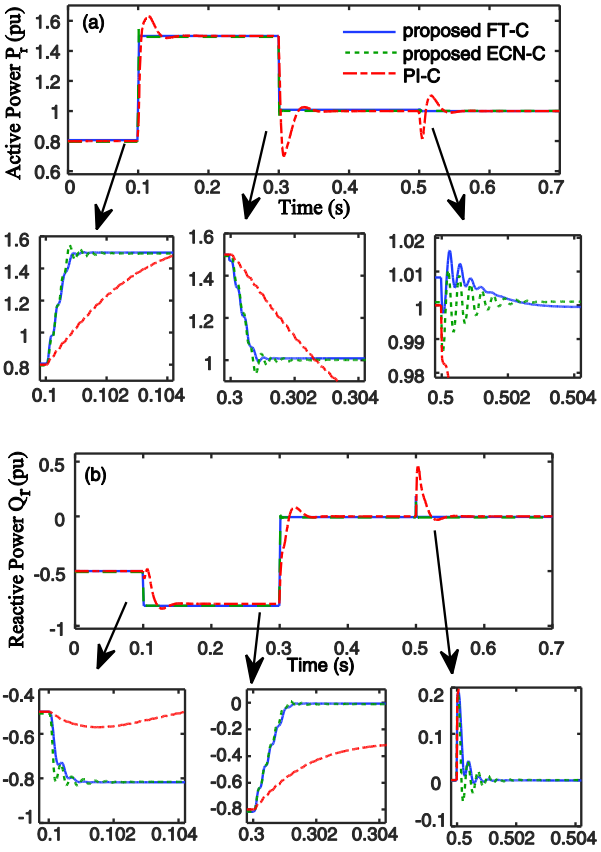

Fig. 3. Power flow through the transmission line with HPFC, using difference controllers. (a) Delivered active power (P_r), (b) delivered reactive power (Q_r).

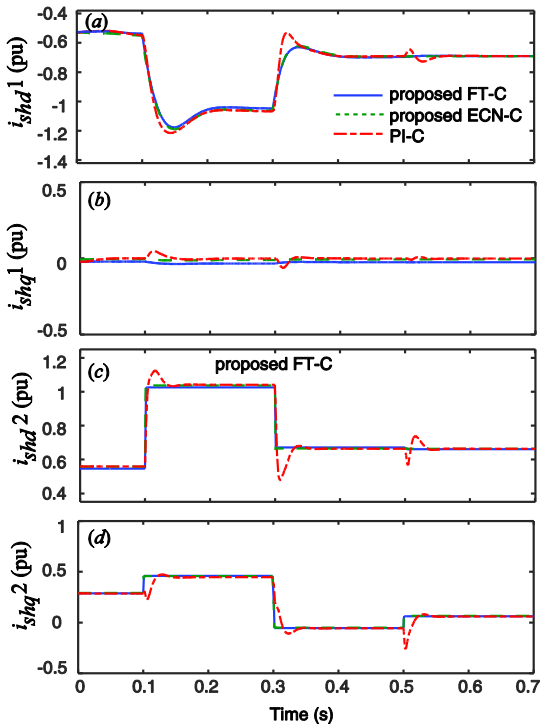

Fig. 4. Injected current of the converters; (a) VSC1 d-axis current, (b) VSC1 q-axis current, (c) VSC2 d-axis current, (d) VSC2 q-axis current.

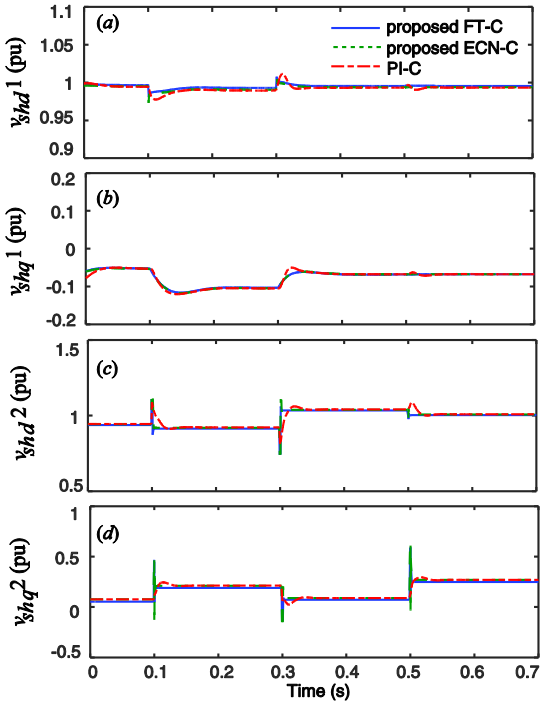

Fig. 5. Controller outputs; (a) VSC1 d-axis voltage, (b) VSC1 q-axis voltage, (c) VSC2 d-axis voltage, (d) VSC2 q-axis voltage.

These performance measures are calculated for the error in tracking the reference power flow, during the time-interval $t_d = 0.3-0.7(s)$. The results are presented in Table IV, which show that the performance of the proposed FT-C is superior compared to ECN-C and PI-C.

Moreover, the control effort $h(u^2)$, where $h(\cdot)$ is defined as Eq. (26), is compared in Table V, for the proposed controllers. Although the control efforts are similar for the designed controllers, FT-C yields improved performance compared to ECN-C and PI-C, regarding the results in Table IV.

Table 4. Measures of controlled HPFC performance

Power	Controller	MISE	MIAE	MITAE
P	FT-C	2.062e-4	4.900e-3	5.059e-4
	ECN-C	2.315e-4	1.600e-3	2.062e-4
	PI-C	3.400e-3	1.950e-3	1.600e-3
Q	FT-C	6.868e-4	7.100e-3	1.200e-3
	ECN-C	8.481e-4	1.130e-3	2.000e-3
	PI-C	7.400e-3	2.570e-3	2.800e-3

Table 5. Control effort

Controller		FT-C	ECN-C	PI-C
VSC2	v_d	1.018	1.022	1.024
	v_q	0.201	0.201	0.200
VSC1	v_d	0.995	0.994	0.993
	v_q	0.068	0.067	0.067

Table 6. Error measures of the discontinuous FT-C

Power	Controller	MISE	MIAE	MITAE
P	DFT-C	6.005e-4	4.500e-3	5.552e-4
Q	DFT-C	1.700e-3	1.070e-2	1.400e-3

The simulation results for the discontinuous FT-C (DFT-C) in Eq. (23) and the causing chattering phenomena are depicted in Fig. 6. It is shown that the reference-tracking would be inaccurate in the presence of chattering. The performance measures for the DFT-C are listed in Table VI. Comparing the performance measures of continuous FT-C with DFT-C, we conclude that FT-C meets the practical requirements since the chattering is removed.

Nominal values of the non-local time-variable parameters are precisely estimated by adaptive affine observer as shown in Fig. 7. Fast response of the used observer makes it suitable for our proposed FT-C. Large gain values are allowable as the observer would be implemented by software. In validation of this issue, it is worth mentioning that the steady state norm 1 of the matrices S_x and S_θ are 0.001.

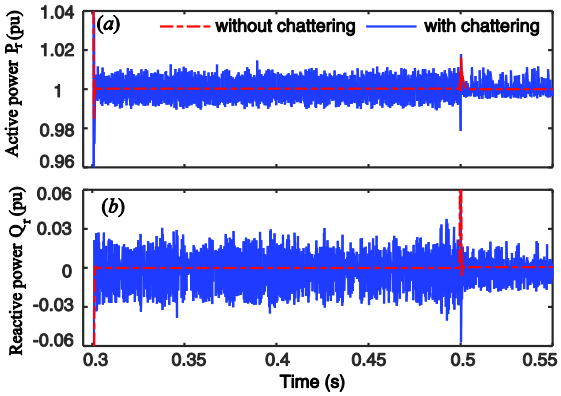

Fig. 6. Impact of chattering phenomena on power flow through the transmission line controlled by discontinuous FT-C (with chattering) and continuous FT-C (without chattering)

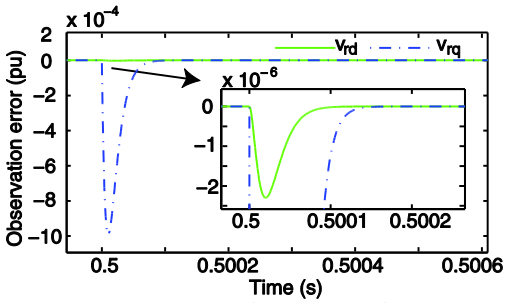

Fig. 7. Estimation error of the observer for non-local parameters.

4.2 Scenario 2 (three-phase short-circuit fault)

In this scenario, the detailed model of three-level VSCs with PWM are used for the HPFC. A three-phase short-circuit fault is applied at the middle of the

parallel transmission line in Fig. 1.

The fault starts at *t=0.2* (s) and lasts for 5 cycles. This fault causes a voltage sag at the receiving end and at the terminals of the HPFC, shown in Fig. 8.

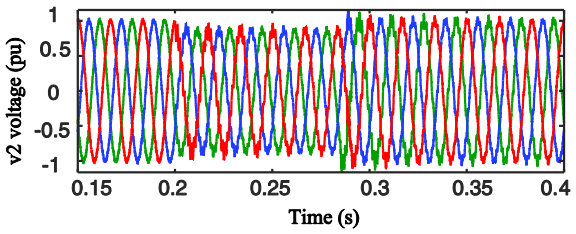

Fig. 8. Voltage sag at the HPFC terminal v_2 caused by the three-phase short circuit fault at the middle of the parallel line.

In order to restore the desired power flow, the voltage sag is compensated by the proposed robust controller and the adaptive observer. The active and the reactive power flow are restored to the pre-fault values immediately, which are not depicted here for briefness. Nonetheless, the control outputs and the VSC output current are presented. Capability of the VSC1 with the proposed controller in regulating the dc link voltage during voltage sag is depicted in Fig. 9. The 3-phase 3-level output voltage of VSC2 is shown in Fig. 10. The 3-level VSC2 with the coupling transformer injects a sinusoidal current, as depicted in Fig. 11. The current magnitude increases during the fault, due to the voltage sag at the terminals of the HPFC. However, the current variation is compensated in the steady state, immediately after the clearance of the fault.

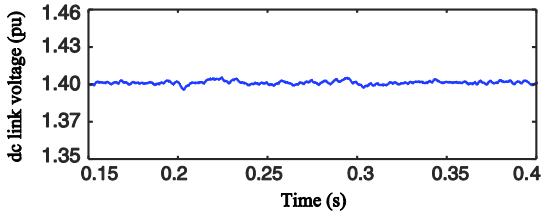

Fig. 9. Controlled dc link voltage of the HPFC with two 3-level back-to-back VSCs.

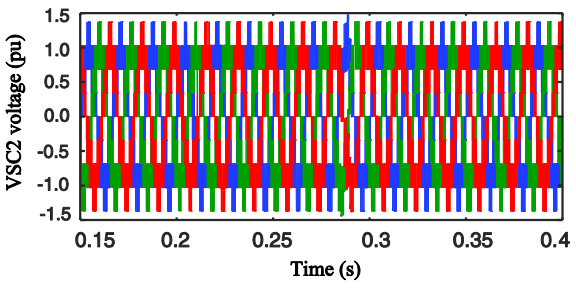

Fig. 10. Output voltage of the 3-level VSC2 during the fault

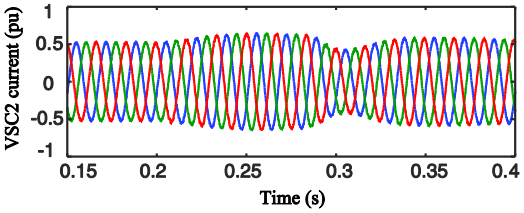

Fig. 11. Output current of the second shunt 3-level VSC2 during the fault

4.3 Impact of the control parameters on the system response

The parameters of the controllers are tuned with respect to the Lyapunov stability criteria, and the convergence time of the states considering the desired settling time Eq. (21). In order to satisfy the Lyapunov inequalities Eqs. (18) and (20), the control parameters are designed as the following.

The control gains μ and β are selected to be positive real values; the fractional power α is limited to the interval (0,1), for finite-time convergence; the robustness gain g_m is greater than the aggregated perturbations norm $\| g_i \|$, which is calculated in detail in the Appendix A, for parameter variations.

Notably, violation of the mentioned conditions may result in instability due to Lyapunov analysis. As stated in Remark 1, larger control gain, and smaller fractional power, shorten the settling time which are also depicted in Figs. 12 (a) and (b), respectively. The impact of the control gain and the fractional power on the settling time Eq. (21) are depicted in Fig. 12.

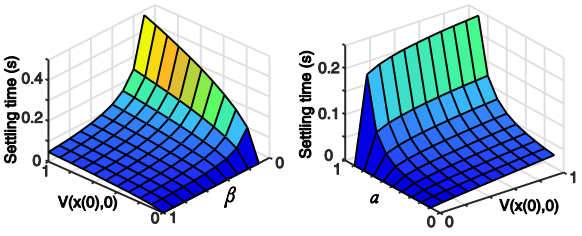

Fig. 12. Impact of control gain (β), fractional power (α) and the initial Lyapunov function on the settling time; Left: impact of β with fixed $\alpha = 0.5$; Right: Impact of α with fixed $\beta = 1$.

However, the high gain yields undesirable response and may cause instability, in the presence measurement noise and delays. Moreover, the impact of the time-delayed controller on system response is demonstrated in Fig. 13, using frequency response analysis. The delay in the control law is caused by the

remote measurements. The Bode diagram is shown for different control gains (i.e. k=1, 10, 100) and time delays (i.e. τ=10, 100 (*ms*)). As shown, the phase margin decreases while increasing the control gain. The gain margin is negative and thus the system is unstable for the time delay 100 (*ms*) with the control gain 100 and higher.

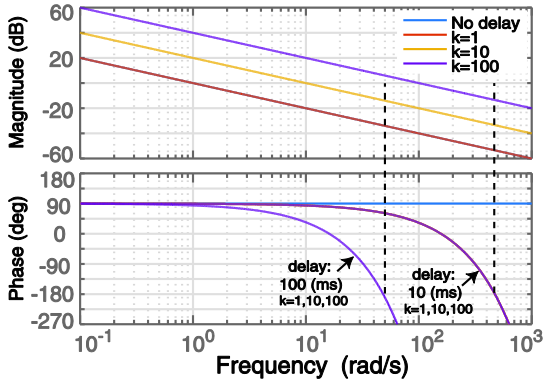

Fig. 13. Bode diagram of the closed-loop system with time-delayed controller; k is the control gain (i.e. β).

4.4 Power flow control between two busses of the modified IEEE 30 bus test system with HPFC

Here, we assume an HPFC is installed between the busses 1 and 2 of the IEEE 30 bus test system [44, 46], and a wind farm is connected to the grid as illustrated in Fig. 16 (Appendix B). The active and reactive power delivered to bus 2 from bus 1 (i.e. the receiving end) are $P_r = -P_{21} = 1.722(pu)$ and $Q_r = -Q_{21} = -0.326(pu)$, without the HPFC and the wind farm.

The varying wind generation, disturbs the original power flow pattern, and requires online regulation of the bus voltage phase and magnitude. In order to compensate for the varying wind generation, and preserve the pre-scheduled power flow pattern, the HPFC is utilized to control the power output of the slack bus (bus 1) without modifying the voltage phase and magnitude of bus 1.

The wind farm consists permanent magnet synchronous generators which are connected to the grid through back-to-back VSC interfaces. The aggregated output wind generation is depicted in Fig. 14 for this case study. The reactive power consumed by the wind farm is assumed to be approximately a constant value of 0.01 MVAR.

As shown in Fig. 15, the HPFC injects the residual power to deliver the constant pre-scheduled power $P_r = 1.722(pu)$ and $Q_r = -0.326(pu)$ to compensate for the varying wind power generation. The output reference current for the HPFC is altered consequently to consider the wind generation.

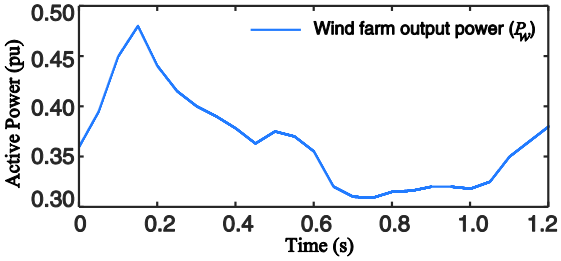

Fig. 14. Aggregated active power generation by the wind farm.

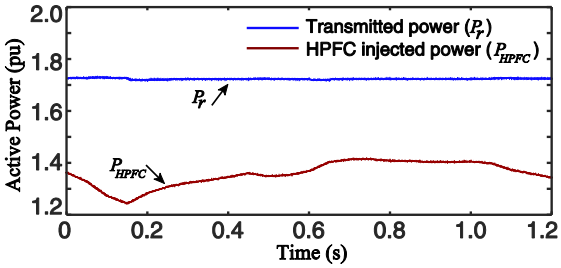

Fig. 15. Power flow control with an HPFC installed between bus 1 and 2 of the IEEE 30 bus test system, to compensate for the varying wind generation.

5. CONCLUSIONS

In this study, a robust decentralized controller is designed based on CLF method to control the power flow in a power system using a new configuration of the conventional UPFC named as HPFC. The proposed FT-C stabilizes the system states in a particular known time, is robust against uncertainties and rejects disturbance. Besides, the power flow control requires online and persistent measurement of the receiving end voltage, which needs high-bandwidth communication. Decentralization of the suggested controller, using an adaptive observer, eliminates the need for persistent communication of the remote measurements, and enhances the system to be robust against communication loss and delays. Lyapunov stability, finite-time convergence and robustness of the CLF-based FT-C is proved both in theory and by numerical simulations, which are validated on a perturbed power system. The proposed FT-C yields superior results in comparison with the conventional nonlinear and PI control in convergence time, tracking error, and overshoot magnitude for power flow applications. It is also illustrated that the controlled system rejects the disturbances and is

robust against uncertainties. The impact of the high control gains and communication delays are shown using Bode diagrams.

APPENDIX A

There would be numerous reasons leading to changes in parameters of a system including external and internal disturbances. Deviation of parameters can be expressed as:

$$A = A_0 + \Delta A, v = v_0 + \Delta v, B = B_0 + \Delta B \quad (33)$$

where subscript *0* denotes the nominal values. Substituting Eq. (33) into Eq. (8) and augmenting the external bounded disturbance (d), we have:

$$\begin{aligned} \dot{e} &= (A_0 + \Delta A)e - (A_0 + \Delta A)x^* \\ &\quad -(v + \Delta v) - (B_0 + \Delta B)u - d - g(t,x) \end{aligned} \quad (34)$$

Comparing Eq. (8) with Eq. (34), we have:

$$g = \Delta A(t)x(t) + \Delta v(t) + \Delta B(t) \times u(x,t) + d(t) \quad (35)$$

Accordingly, the boundary of the uncertainties and thus the required maximum value of g_m in proposed controllers, Eqs. (14) and (23), are estimated by Eq. (35). In the following, we calculate the minimum required g_m for relative variations of the system parameters. Assume, the variations are fractions of the nominal values as:

$$\Delta A = \Omega_A A_0, \Delta v = \Omega_v v_0, \Delta B = \Omega_B B_0 \quad (36)$$

Suppose, as a worst case, σ is the relative maximum increase of the parameters except for L_{sh}, which have minimum decrease by ς.Thus, the variation factors in Eq. (30) are calculated as:

$$\Omega_A = \Omega_v = (\sigma + \varsigma)(1-\varsigma)^{-1} \mathrm{I}_4, \Omega_B = \varsigma(1-\varsigma)^{-1} \quad (37)$$

In order to secure the stability of the proposed controllers we have to set g_m larger than the aggregated disturbances and perturbations, as:

$$g_m \geq \max\{|\Omega_A A_0 x + \Omega_v v_0 + \Omega_B B_0 u + d|\} \quad (38)$$

The max function in Eq. (38) is the motive to choose σ and ς as the maximum increase and minimum decrease percentage, respectively. Consequently, calculating g_m is straightforward since Eq. (38) consists nominal, known and measurable values.

APPENDIX B

The modified IEEE 30 bus test system, with an HPFC and a wind farm is shown in Fig. 15. The complete data of the power system is available in the literature [44, 46] and is not given here for briefness. Specifications of the HPFC and the wind generation are given in Fig. 1 (b) as well as Table I, and the section 4.4, respectively.

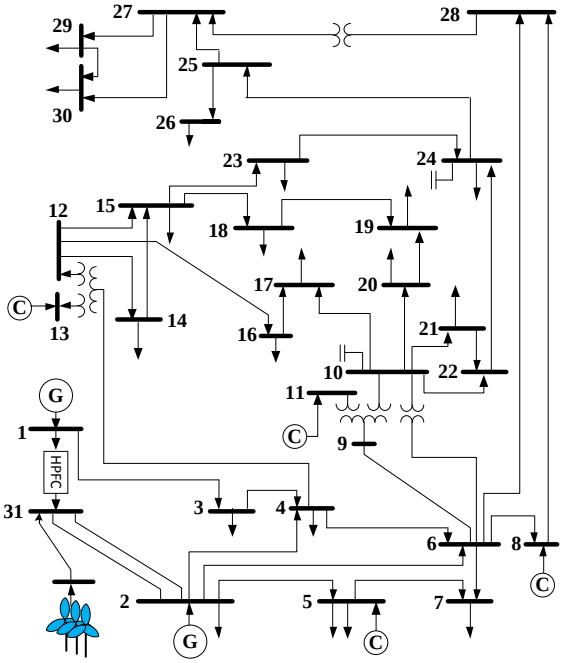

Fig. 16. Single-line diagram of the modified IEEE 30 bus system with an HPFC and a wind farm; G denotes the generators, and C denotes the synchronous condensers.

REFERENCES

[1] S. Kamel, F. Juradoa, and J. A. P. Lopes, "Comparison of various UPFC models for power flow control" *Electr. Power Syst. Res.*, vol. 121, pp. 243-251, 2015.

[2] G. S. Ilango, C. Nagamani, A. V. S. S. R. Sai, and D. Aravindan, "Control algorithms for control of real and reactive power flows and power oscillation damping using UPFC" *Electr. Power Syst. Res.*, vol. 79, pp. 595-605, 2009.

[3] L. Gyugyi, "A unified power flow control concept for flexible AC transmission systems" *IEEE Proc. C Gener. Transm. Distrib.*, vol. 139, no. 4, pp. 323-331, 1992.

[4] S. A. Al-Mawsawi, "Comparing and evaluating the voltage regulation of a UPFC and STATCOM" *Int. J. Electr. Power Energy Syst.*, vol. 25, pp. 735-740, 2003.

[5] E. Gholipour and S. Saadate, "Improving of transient stability of power systems using UPFC" *IEEE Trans. Power Delivery*, vol. 20, no. 2, pp. 1677-1682, 2005.

[6] A. M. Shotorbani, A. Ajami, M. P. Aghababa, and S. H. Hosseini, "Direct Lyapunov theory-based method for power oscillation damping by robust finite-time control of unified power flow controller" *IET Gener. Transm. Distrib.*, vol. 7, pp. 691-699, 2013.

[7] J. Guo, M. L. Crow, and J. Sarangapani, "An improved UPFC control for oscillation damping" *IEEE Trans. Power Syst.*, vol. 14, pp. 288-296, 2009.

[8] N. Bigdeli, E. Ghanbaryan, and K. Afshar, "Low frequency oscillations suppression via CPSO based damping controller" *J. Oper. Autom. Power Eng.*, vol. 1, pp. 22-32, 2013.

[9] M. R. Esmaili, A. Khodabakhshian, and M. Bornapour, "A new coordinated design of UPFC controller and PSS for improvment of power system stability using CPCE algorithm" *Proc. IEEE Electr. Power Energy Conf.*, Ottawa, pp. 1-6, 2016.

[10] L. Wang, H.W. Li, and C.T. Wu, "Stability analysis of an integrated offshore wind and seashore wave farm fed to a power grid using a unified power flow controller" *IEEE Trans. Power Syst.*, vol. 28, pp. 2211-2221, 2013.

[11] W.M. Lin, K.H. Lu, and T.C. Ou, "Design of a novel intelligent damping controller for unified power flow controller in power system connected offshore power applications" *IET Gener. Transm. Distrib.*, vol. 9, pp. 1708-1717, 2015.

[12] A. Mohanty, S. Patra, and P. K. Ray, "Robust fuzzy-sliding mode based UPFC controller for transient stability analysis in autonomous winddiesel-PV hybrid system" *IET Gener. Transm. Distrib.*, vol. 10, pp. 1248-1257, 2016.

[13] M. Firouzi, G. B. Gharehpetian, and B. Mozafari, "Power-flow control and short-circuit current limitation of wind farms using unified interphase power controller" *IEEE Trans. Power Delivery*, vol. 32, pp. 32-71, 2017.

[14] M. A. Sayed and T. Takeshita, "Line loss minimization in isolated substations and multiple loop distribution systems using the UPFC" *IEEE Trans. Power Electron.*, vol. 29, pp. 5813-5822, 2014.

[15] A. R. Ghahnavieh, M. Fotuhi-Firuzabad, and M. Othman, "Optimal unified power flow controller application to enhance total transfer capability" *IET Gener. Transm. Distrib.*, vol. 9, pp. 358-368, 2015.

[16] J. Z. Bebic, P. W. Lehn, and M. R. Iravani, "The hybrid power flow controller a new concept for flexible AC transmission" *Proc. IEEE Power Eng. Soc. Gen. Meeting*, pp. 1-6, 2006.

[17] A. K. Sadigh, M. T. Hagh, and M. Sabahi, "Unified power flow controller based on two shunt converters and a series capacitor" *Electr. Power Syst. Res.*, vol. 80, pp. 1511-1519, 2010

[18] A. Shukla, A. Ghosh, and A. Joshi, "Static shunt and series compensation of an SMIB system using flying capacitor multilevel inverter, " *IEEE Trans. Power Delivery*, vol. 20, pp. 2613-2622, 2005.

[19] D. Soto and T. C. Green, "A comparison of high-power converter topologies for the implementation of FACTS controllers, " *IEEE Trans. Indus. Electron.*, vol. 49, pp. 1072-1080, 2002.

[20] S. Yang, D. Gunasekaran, Y. Liu, U. Karki, and F. Z. Peng, "Application of transformer-less UPFC for interconnecting synchronous AC grids, " *Proc. IEEE Energy Convers. Congr. Expos.*, Montreal, 2015, pp. 1-6.

[21] F. Z. Peng, Y. Liu, S. Yang, S. Zhang, D. Gunasekaran, and U. Karki, "Transformer-less unified power-flow controller using the cascade multilevel inverter, "*IEEE Trans. Power Electron.*, vol. 31, pp. 5461-5472, 2016.

[22] S. Yang, Y. Liu, X. Wang, D. Gunasekaran, U. Karki, and F. Z. Peng, "Modulation and control of transformerless UPFC, " *IEEE Trans. Power Electron.*, vol. 31, pp. 1050-1063, 2016.

[23] Y. Liu, S. Yang, X. Wang, D. Gunasekaran, U. Karki, and F. Z. Peng, "Application of transformer-less upfc for interconnecting two synchronous AC grids with large phase difference" *IEEE Trans. Power Electron.*, vol. 31, pp. 6092-6103, 2016.

[24] A. M. Shotorbani, A. Ajami, S. G. Zadeh, M. P. Aghababa, and B. Mahboubi, "Robust terminal sliding mode power flow controller using unified power flow controller with adaptive observer and local measurement, " *IET Gener. Transm. Distrib.*, vol. 8, pp. 1712-1723, 2014.

[25] A. Ajami, A. M. Shotorbani, and M. P. Aagababa, "Application of the direct Lyapunov method for robust finite-time power flow control with a unified power flow controller, " *IET Gener. Transm. Distrib.*, vol. 6, pp. 822-830, 2012.

[26] T. T. Ma, "P-Q decoupled control schemes using fuzzy neural networks for the unified power flow controller, " *Int. J. Electr. Power Energy Syst.*, vol. 29, pp. 748-758, 2007.

[27] J. Monteiro, J. F. Silva, S. F. Pinto, and J. Palma, "Linear and sliding-mode control design for matrix converter-based unified power flow controllers, " *IEEE Trans. Power Electron.*, vol. 29, pp. 3357-3367, 2014.

[28] M. J. Kumar, S. S. Dash, A. S. P. Immanuvel, and R. Prasanna, "Comparison of FBLC (feed-back linearization) and PI-controller for UPFC to enhance transient stability, " *Proc. Int. Conf. Comput. Commun. Electr. Technol.*, 2011, pp. 1-6.

[29] B. Lu and B. T. Ooi, "Unified power flow controller (UPFC) under nonlinear control, " *Proc. PCC-Osaka Power Convers. Conf.*, 2002, pp. 1-6.

[30] G. S. Ilango, C. Nagamani, and D. Aravindan, "Independent control of real and reactive power flows using UPFC based on adaptive back stepping, " *Proc. IEEE Reg. 10 Conf.*, Hyderabad, 2008, pp. 1-6.

[31] S. Mehraeen, J. Sarangapani, and M. L. Crow, "Novel dynamic representation and control of power systems with FACTS devices, " *IEEE Trans. Power Syst.*, vol. 25, pp. 1542-1554, 2010.

[32] H. Alasooly and M. Redha, "Optimal control of UPFC for load flow control and voltage flicker elimination and current harmonics elimination, " *Comput. Math. Appl.*, vol. 60, pp. 926-943, 2010.

[33] A. Rajabi-Ghahnavieh, M. Fotuhi-Firuzabad, and M. Othman, "Optimal unified power flow controller application to enhance total transfer capability, " *IET Gener. Transm. Distrib.*, vol. 9, pp. 358-368, 2015.

[34] S. A. Taher, S. Akbari, A. Abdolalipour, and R. Hematti, "Design of robust decentralized control for UPFC controller based on structured singular value, " *Am. J. Appl. Sci.*, vol. 5, no. 10, pp. 1269-1280, 2008.

[35] F. Shalchi, H. Shayeghi, and H. A. Shayanfar, "Robust control design for UPFC to improve damping of oscillation in distribution system by H_2 method, " *Proc. 16th Conf. Electr. Power Distrib. Networks*, Bandar Abbas, 2011.

[36] M. M. Farsangi, Y. H. Song, W. L. Fang, and X. F. Wang, "Robust FACTS control design using the H/sub/spl infin loop-shaping method," *IEE Proc. Gener. Transm. Distrib.*, vol. 149, pp. 352-358, 2002.

[37] M. Januszewski, J. Machowski, and J. W. Bialek, "Application of the direct Lyapunov method to improve damping of power swings by control of UPFC, " *IEE Proc. Gener. Transm. Distrib.*, pp. 252-260, 2004.

[38] S. G. Nersesov, W. M. Haddad, and Q. Hui, "Finite-time stabilization of nonlinear dynamical systems via control vector Lyapunov functions, " *J. Franklin Inst.*, vol. 345, pp. 819-837, 2008.

[39] S. Yu, X. Yu, B. Shirinzadeh, and Z. Man, "Continuous finite-time control for robotic manipulators with terminal sliding mode, " *Autom.*, vol. 41, pp. 1957-1964, 2005.

[40] A. G. L. H. Huerta, J.M. Canedo, "Robust multi-machine power systems control via high order sliding modes, " *Electr. Power Syst. Res.*, vol. 81, pp. 1602-1609, 2011.

[41] H. Huerta, A. G. Loukianov, and J. M.Cañedo, "Multimachine power-system control: integral-sm approach, " *IEEE Trans. Ind. Electron.*, vol. 56, pp. 2229-2236, 2009.

[42] V. I. Utkin, J. Guldner, and J. Shi, *Sliding Mode Control in Electromechanical Systems*. London: Taylor & Francis, 1999.

[43] G. Besancon, J. D. Leon–Morales, and O. Huerta–Guevara, "On adaptive observers for state affine systems, "*Int. J. Control*, vol. 79, pp. 581-591, 2006.

[44] H. Saadat, *Power System Analysis*, Second Edition ed.: McHraw-Hill, 2002.

[45] W. C. Schultz and V. C. Rideout, "Control system performance measures: Past, present, and future" *IRE Trans. Autom. Control*, vol. AC-6, pp. 22-35, 1961.

[46] R. Kazemzadeh, M. Moazen, R. Ajabi-Farshbaf, and M. Vatanpour, "STATCOM optimal allocation in transmission grids considering contingency analysis in OPF using BF-PSO algorithm, " *J. Oper. Autom. Power Eng.*, vol. 1, no. 1, pp. 1-11, 2013.